JOURNAL OF MATERIALS SCIENCE **35** (2000) 2769–2777

Effect of soft substrate on the indentation damage in silicon carbide deposited on graphite

KEE SUNG LEE, JI YEON PARK, WEON-JU KIM, MIN YOUNG LEE, CHOONG HWAN JUNG, GYE WON HONG
Functional Materials, Korea Atomic Energy Research Institute, Taejon 305-353, South Korea
E-mail: jypark@nanum.kaeri.re.kr

Indentation-induced damage is investigated in silicon carbide (SiC) deposited on graphite substrate. The SiC films have been grown by LPCVD (Low Pressure Chemical Vapor Deposition) method using MTS (CH_3SiCl_3) as a source gas and H_2 as a diluent gas to provide highly dense deposited layer and strong interfacial bonding. The elastic-plastic mismatch is very high to induce distinctive damages in the coating and the substrate layer. The specimens with various coating thicknesses are prepared by changing CVD condition or mechanical polishing. Indentation damages with different sizes are introduced by controlling indentation load in Nanoindentation, Vickers indentation and Hertzian indentation test. Basic mechanical properties such as hardness, toughness, elastic modulus are evaluated against coating thickness. Mechanical properties are sensitive to the indentation load and coating thickness. The results indicate that coating thickness has a vital importance on the design of hard coating/soft substrate system because the soft substrate affects on the mechanical properties.

1. Introduction

Whenever two materials touch each other, the surfaces may undergo contact stresses [1, 2]. Contact stresses are influenced by a load of one material on the other one over contact areas. These stresses may cause deformation or fracture onto the weaker material. These kinds of contact stresses are very important in brittle ceramics because small damage introduces critical flaws near the surface region, leading to catastrophic failure of material [1–4]. Real ceramic products contain various types of flaws such as cracks, pores, inclusions and segregations whether they are deliberately introduced or not. It is inevitable that the flaws are introduced during shaping or in the practical use. Therefore, over several decades, the strategy of development of high-reliability ceramics has changed from elimination of flaws [5, 6] to flaw-insensitivity [6, 7]. "Flaw tolerance," "damage tolerance," or "flaw-insensitivity" has become an important property that is defined as follows: the strength of a material is not degraded even under the applied high or multiple damages.

Some prior studies on laminates or bilayer systems have foreshadowed the possibility of damage-tolerant ceramics [8–11]. Most of them consist of more than two layers with different compositions. Generally, hard ceramics cannot be matched with high toughness. According to recent microstructure development to increase the damage tolerance of brittle ceramics, it is well known that large grain, elongated grain, weak and residual compressive grain boundaries are profitable [3]. However, this microstructure control may cause the degradation of wear and fatigue properties [12, 13]. Therefore bilayer structure can render a solution to develop the materials exhibiting both high hardness and high toughness at the same time. These laminates are fabricated by various processing methods such as tape casting, CVD (chemical vapor deposition), powder packing, slurry dipping and electrophoretic deposition [14]. The advantages of these systems are that mechanical, electrical, or thermal properties can be tailored by combination of layers with different properties for specific applications. Proper designs of layer geometry, microstructure and composition lead to significant improvement in damage tolerance [9–11, 14, 15].

One example of a bilayer material is the SiC deposited graphite with a hard coating/soft substrate system. While a hard coating layer provides high hardness, a soft but tough underlayer provides high toughness by appropriate design. The SiC-coated graphite structure has been applied to refractory compounds with high hardness, chemical stability and high oxidation resistance. It is also used for radiation resistant material due to a low induced radioactivity or in the semiconductor industry due to a low friction coefficient [16, 17].

In designing these kinds of layer systems, controls of design parameters such as residual stress, interfacial strength and elastic/plastic mismatch are very important [8, 10, 11]. One layer should be residual compressive stress to diminish the driving force of crack growth by controlling the difference of thermal expansion coefficients between two layers during the fabrication of laminates or coating systems. Interfacial strength is also important because the strength of interface is less than that of layer monolith, which causes an interfacial

delamination fracture [18, 19]. Recent studies show that elastic/plastic mismatch and coating thickness are very important parameters in designing damage-tolerant ceramics [11, 15]. Sometimes, applied damage can affect the substrate layer as well as the coating layer in the practical use of ceramic products. Some studies on coating failure indicate that the substrate highly affects the fracture of the coating layer [10, 15, 20].

In this study we investigate the effect of substrate on the coating damage in the practical coating system of SiC deposited graphite using static indentation methods such as nanoindentation, microhardness indentation and Hertzian indentation. We shall show that greater damage is more influenced by soft graphite substrates. The result of crack suppression on a very thin coating suggests the prospect of designing a layer structure for high damage tolerance.

2. Experimental procedure

2.1. Fabrication and characterization of layered structure of CVD-SiC

Polycrystalline β-SiC layers were deposited in a hot wall LPCVD (low pressure chemical vapor deposition) horizontal reactor. The furnace temperature, 1200°C, was uniformly maintained across all zones, and the pressure, 5 torr, was measured at the reactor outlet. We used the titled graphite (tilted angle $\approx$10°) as a supporter by considering the uniformity of gas flow. Prepolished isotropic graphite (25 mm diameter $\times$ 3 mm thickness) was used as a substrate. Methyltrichlorosilane (MTS) was saturated into hydrogen gas. Gas flow rates were controlled by MFC (mass flow controller, Tylan Co., USA) while maintaining the temperature of the bubbler at 0°C. The reaction was performed for 1–3 h with constant ratio of MTS : $H_2 = 1 : 4$.

CVD coated graphite systems with different coating thicknesses were prepared in order to elucidate the effect of the substrate layer. Coating thickness was controlled during CVD processing or by mechanical grinding.

The phase of the coating layer was identified by X-ray diffractometry (XRD), and the microstructure was observed by scanning electron microscopy (SEM). Surfaces of deposited materials were polished up to 1 μm finish to check the porosity by optical microscopy. Coating thicknesses were also confirmed by optical microscopy or SEM. The thermal expansion coefficients of layer monoliths were measured with a dilatometer.

2.2. Static indentation test

We introduced damage in various sizes to know the effect of the substrate. Small sized damage is introduced at a lower load by nanoindentation or microhardness indentation. A large sized damage is introduced at a higher load by Hertzian indentation. Some of the indentation damage is *in-situ* observed by optical microscopy, and mechanical properties such as hardness, toughness and elastic modulus are characterized. Coating thickness is in the range of 20 to 70 μm. Static indentation tests were made on these specimens at various loads to determine deformation and fracture responses.

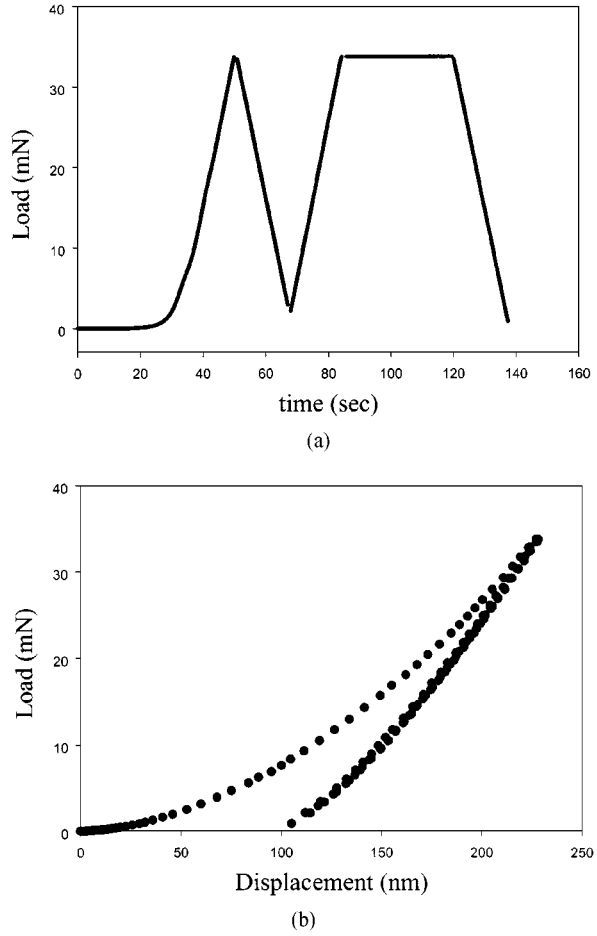

Figure 1 Typical diagram of (a) load-time sequence and (b) load-displacement curve in nanoindentation test.

2.2.1. Nanoindentation test

Nanoindentations were performed using a three-sided pyramidal diamond indenter, which has recently become a widely used technique to evaluate the hardness and elastic modulus of thin films [21–23]. These properties can be obtained from a load-displacement curve without observing submicron indentations. Indentation loads were 33 mN and 5 mN with indentation depths of 300 and 100 nm, respectively. Six indentations were made at each load. All indentations were performed using a load-time sequence, as shown in Fig. 1a. After holding for 30 sec, the indenter was first loaded and unloaded for one time with an unloading finish at 10% of the peak load to maintain contact between indenter and specimen. After that, the load was increased again and maintained for 40 sec to remove time-dependent plastic effect [21], and then the specimen was fully unloaded.

Hardness and elastic modulus were measured from load-displacement curves. The typical load-displacement curve obtained is shown in Fig. 1b. Elastic modulus is related to the slope of the unloading curve of the load-displacement curve. Experimentally measured stiffness is defined as following [21]:

$$S = \frac{\mathrm{d}P}{\mathrm{d}h} = 2Er(A)^{1/2}(\pi)^{-1/2} \qquad (1)$$

where A is the projected area of the elastic contact. The contact area at peak load is determined by the geometry

of the indenter and the depth of the contact. So, we can easily obtain the elastic modulus from the above equation. Hardness is calculated from

$$H = \frac{P_{\max}}{A} \tag{2}$$

Where A is the projected area of contact at peak load.

2.2.2. Microhardness and Vickers indentation test

Conventional microhardness and Vickers indentation was performed on the polished surfaces of each specimen. The indentation load varied from 0.5 N to 20 N to induce different sizes of damage on the topside of the coated layer with different coating thicknesses. Hardness, H, and toughness, T_o, were measured using following equations [24, 25]:

$$H = 1.854\frac{P}{d^2} \tag{3}$$

Where P is the indentation load and d is the diagonal length of surface damages.

$$T_o = \frac{\chi P}{c^{3/2}} \tag{4}$$

Where $\chi = 0.016\ (E/H)^{1/2}$, E is the elastic modulus and c is the indentation crack length. Toughness was evaluated from the radial crack length produced at the indentation load $P = 2$ N. Surface damages were observed by optical microscopy or SEM.

2.2.3. Hertzian indentation test

Hertzian indentations were made using tungsten carbide (WC) spheres with radius $r = 3.18$ mm, at peak load up to $P = 500$ N. Hertzian indentation using a spherical indenter is a very simple and powerful technique to evaluate the damage-tolerant ceramics [26–29]. The indented surfaces were gold coated for measuring the size of the contact zone and examined by optical microscopy. Measurements of contact radius a (made visible by coating surface with gold film) at each given load P and sphere radius r enabled calculation of indentation stress, $p_o = P/\pi a^2$, and indentation strain, a/r, for the construction of an indentation stress-strain curve. Elastic modulus E was evaluated from the initial slope of indentation stress-strain curves, where E is derived from the following equation [3]:

$$p_o = \left(\frac{3E}{4\pi k}\right)\left(\frac{a}{r}\right) \tag{5}$$

where $k = 9/16\{(1-\nu^2) + (1-\nu_s^2)(E/E_s)\}$ a dimensionless coefficient, E and ν, E_s and ν_s, Young's modulus and Poisson's ratio of the SiC and WC indenter, respectively. The slope of the indentation stress-strain curve corresponds to $3E/4\pi k$.

Indentations were made on the top surface of each specimen with a different coating thickness. The same indentation load $P = 50$ N was applied. Ring crack and surface impressions were observed by optical microscopy in Nomarski illumination. A serial sectioning test by polishing away from the top indented surface was performed to check the damage pattern formed at the fixed indentation load.

3. Results

3.1. Basic properties of layer materials

The basic characteristics of the coating and the substrate material used in this study are compared with each other in Table I. Hardness and elastic modulus are average values measured from nanoindentation or microhardness indentation tests. Silicon carbide is much harder and stiffer, but on the other hand, graphite shows very soft properties. It is remarkable that the two layers show large differences in hardness and elastic modulus. However, the thermal expansion coefficient does not show much difference between the two materials even if that of silicon carbide is a little bit higher.

Examinations of the polished specimens revealed that as-deposited silicon carbide layers were highly dense. Pores were not observed in the coating layer deposited in this study. The as-deposited silicon carbide layers consisted of stoichiometric compositions and there were no polytypes except for β-SiC. The plane of preferred orientation was (111) plane for the polycrystalline SiC coating layers.

Fig. 2 shows the typical microstructure of the top SiC coating layer examined by SEM. The micrograph

TABLE I Comparison of basic characteristics between SiC and graphite materials

Characteristics	Silicon carbide	Graphite
Hardness (GPa)	46	0.95
Toughness (MPa $m^{1/2}$)	3.84	<1.0
Elastic modulus (GPa)	464	11
Thermal expansion coefficient, $\alpha(\times 10^{-6}/^{\circ}C)$	4.8	4.5
Bulk density (g/cm^3)	3.21	1.83
Crystal phase	β-SiC	

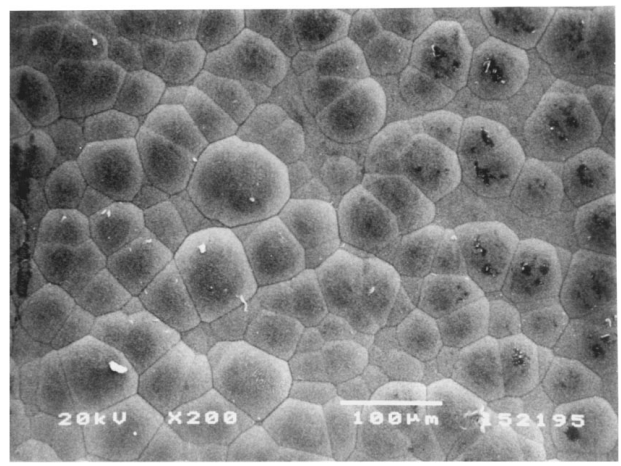

Figure 2 Typical scanning electron micrograph of the surface morphology of as-deposited layer at 1200°C for 3 h.

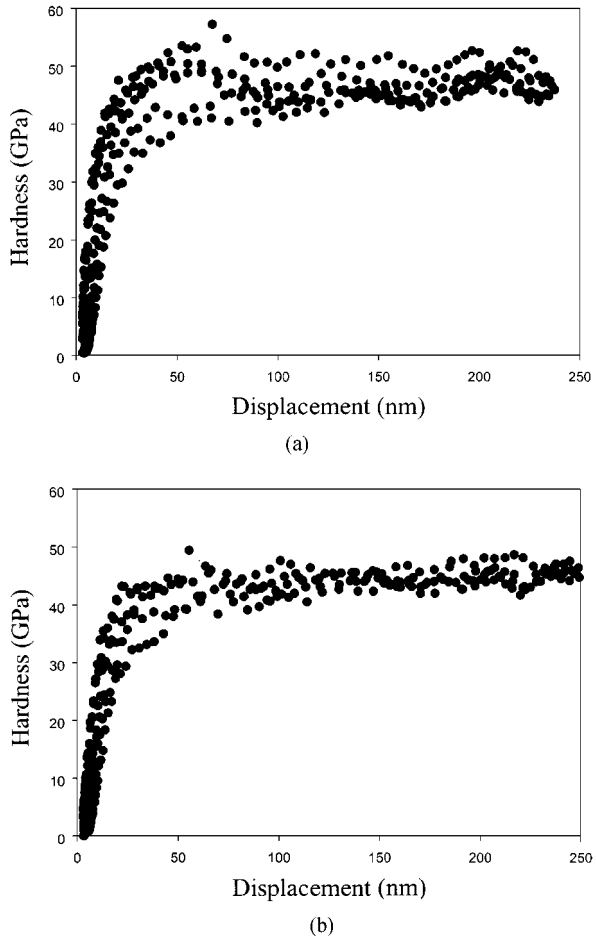

Figure 3 Hardness as a function of displacement in nanoindentation test on the SiC/graphite with different coating thickness; (a) $d = 70$ μm and (b) $d = 50$ μm.

shows that smooth and rounded-grown structure with grain sizes of 25–100 μm are uniformly deposited at the deposition condition.

3.2. Evaluation of hardness

Hardness was evaluated from nanoindentaion or microhardness indentation on specimens with different coating thicknesses. A small indentation load was applied by nanoindentation and relatively larger indentation load was applied by microhardness indentation. Two specimens with different coating thicknesses were prepared for indentations. Fig. 3 shows the hardness results of specimen with coating thicknesses, $d = 70$ μm and 50 μm from nanoindentation, respectively. All hardness data shows relatively constant and similar values to each other after 50 nm indenter penetration, $\approx$46 GPa. The hardness data before 50 nm of displacement are included in the region influenced by Hertzian elastic stress, where we can ignore the exact hardness values. As shown in Fig. 3, hardness makes no difference between the two specimens with different coating thickness.

However, as the indentation load increases, the hardnesses of the two specimens show discrepancy. Fig. 4 shows the variation of hardness according to the indentation load for the specimens with different coating thicknesses. The hardnesses of both specimens show a

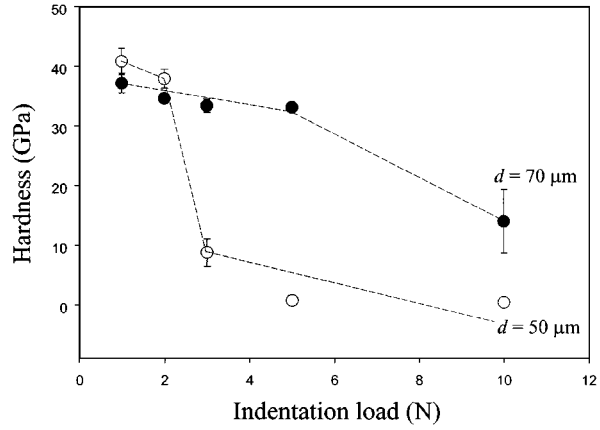

Figure 4 Hardness as a function of indentation load in microhardness test of SiC/graphite at a coating thickness of 50 μm and 70 μm. Note the more decreasing tendency of hardness in thinner-coated structure.

tendency to decrease as the indentation load increases. However, the decreasing tendency is much higher in thinner deposited specimen. Although there are not much differences at lower indentation loads, $P = 1$ N and 2 N, the hardness abruptly decreases at $P = 3$ N in the specimen with a 50 μm coating thickness. On the other hand, the hardness of the specimen with a 70 μm coating thickness begins to abruptly decrease at a higher indentation load, $P = 10$ N. This result indicates that there exists a critical load at which hardness decreases abruptly, and this critical load is much lower in the specimen with the thinner coating thickness.

The reason for the abrupt hardness decrease can be understood by examination of the indentation impression damage. Fig. 5 represents top views of damage formed at indentation loads $P = 2$ N (Fig. 5a) and $P = 3$ N (Fig. 5b) on the SiC coating layer with a 50 μm thickness. At $P = 2$ N, small indentation flaws are observed with radial cracks due to the brittleness of silicon carbide. As the indentation load increases to $P = 3$ N, the size of the indentation impression abruptly increases. However, in this indentation impression, any radial cracks from the indentation flaws are not observed. Only ring-like cracks are observed around the region of the indentation flaws.

A more detailed SEM examination of the larger indentation impression is shown in Fig. 6. The materials in the center region of the indentation flaw are more pushed away than in the outer region and microfractures of grains have occurred in the indentation region.

3.3. Evaluation of elastic modulus

Elastic modulus of SiC deposited on the graphite substrate was evaluated from nanoindentation and Hertzian indentation. Elastic modulus becomes an important factor when the system is situated under the contact loading. In the fixed contact loading, as strain is constant, elastic modulus acts as a stress onto the material. Especially, in the bilayer system, mismatch between two layers—the coating and the substrate layer—can cause fracture or limit the lifetime of the system [15].

Fig. 7 plots elastic modulus derived from unloading curve of load-displacement curve in nanoindentation

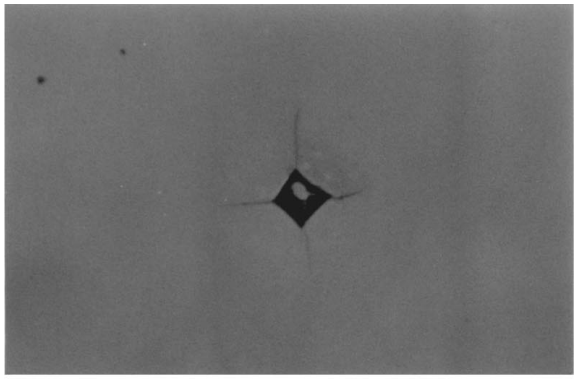

(a)

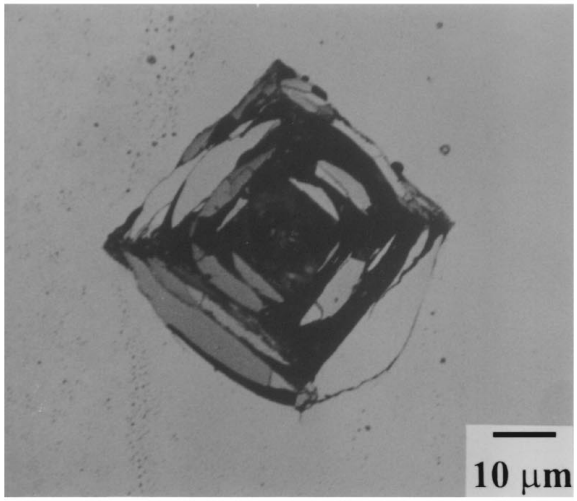

(b)

Figure 5 Surface views of microhardness contact damage in SiC/graphite with coating thickness of 50 μm at indentation load; (a) $P = 2$ N showing radial cracks and (b) $P = 3$ N showing ring cracks.

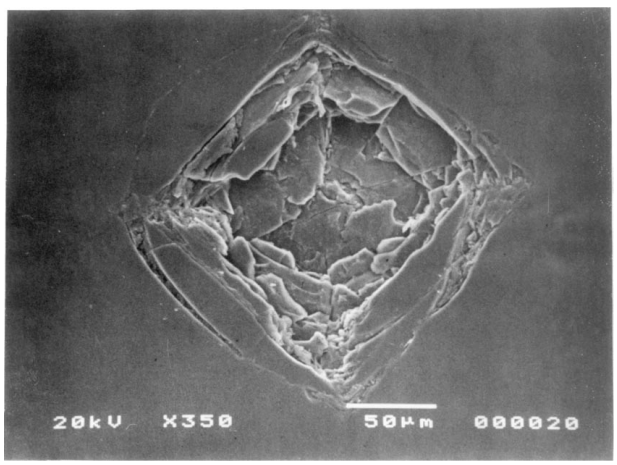

Figure 6 Scanning electron micrograph of microhardness damage of SiC/graphite with coating thickness of 50 μm formed at load of $P = 10$ N.

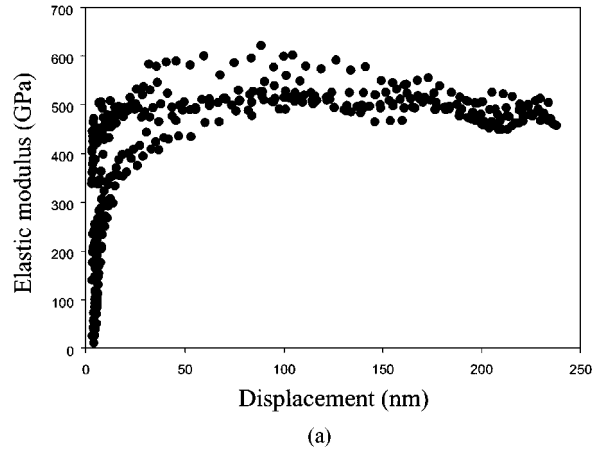

(a)

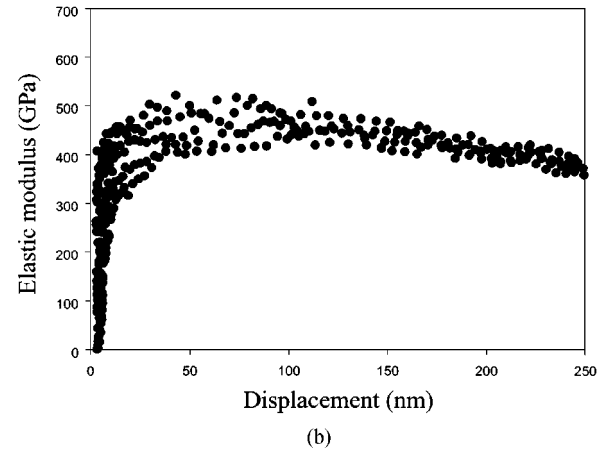

(b)

Figure 7 Elastic modulus as a function of displacement in nanoindentation test on the SiC/graphite with different coating thickness; (a) 70 μm and (b) 50 μm.

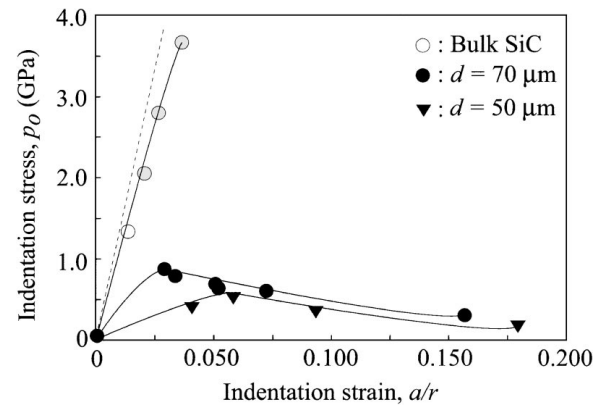

Figure 8 Indentation stress strain curves of SiC/graphite. Inclined dashed line is Hertzian elastic response and open circles correspond to the data of bulk SiC.

test. Average elastic modulus is 460 GPa in the specimen with 70 μm coating thickness and 410 GPa in the specimen with 50 μm coating thickness. Note that the tendency of decrease in elastic modulus with increasing penetration depth at thinner coating thickness.

Indentation stress-strain curves obtained from Hertzian indentation for the two specimens with different coating thickness of 70 and 50 μm, are plotted in Fig. 8, respectively. The dashed line exhibits the linear relation for purely elastic contacts from Hertzian theory [3] of Equation 5. The indentation stress-strain curve of bulk silicon carbide ceramics is included for comparison. The bulk SiC has a homogeneous equiaxed microstructure, thus stress-strain relation of bulk silicon carbide shows brittle and elastic behavior. In this figure, bulk silicon carbide shows relatively elastic behavior at the small indentation strain. However, the indentation stress-strain curves of SiC/graphite systems in this study show complete deviation from ideal linear

relations. Strikingly, the stress-strain response of the coating system varies within the limits of the coating and the substrate curves, according to the relative hardness of coating and substrate [15, 30, 31]. Each stress-strain data initially follows close to that of coating layer monolith, but then passes through a maximum value, and finally approaches the indentation stress-strain curve of the substrate material. This fact indicates that the contact load is initially influenced by the coating layer, and ultimately by the substrate at higher applied indentation load. The maximum point shifts to higher indentation strain as the coating thickness decreases. The values of elastic modulus can be determined for the different coating thickness from the initially linear slopes of indentation stress-strain curves. The exact values are calculated as shown in the section of 2.2.3. Elastic moduli of the two materials are calculated as 41.8 GPa (coating thickness, $d = 70\ \mu$m) and 16.8 GPa (coating thickness, $d = 50\ \mu$m), respectively. These values show large differences when we compare with the elastic modulus values obtained from nanoindentation. In nanoindentation test, submicron-scaled damage region is considered, but in Hertzian test, micrometer-scaled larger damage should be considered. In Hertzian indentation test, larger ($r = 3.18$ mm) indenter was used to induce the surface damage rather than small indenter with submicron scale.

3.4. Toughness and Hertzian contact damage

Toughness was evaluated from crack length after microhardness indentation on the specimens with different coating thicknesses, $d = 50$ and 70 μm. Toughnesses against coating thicknesses are plotted in Fig. 9. The toughness is not largely changed in the range of 40–70 μm coating thicknesses, but below 40 μm, the toughness abruptly increases. This result means that crack suppression occurs at the thinner thickness than some critical thickness.

Fig. 10 shows Hertzian indentation damage made at a load $P = 50$ N with WC sphere radius of $r = 3.18$ mm. Fig. 10a shows the micrographs of top surface damage in the specimen with 70 μm coating thickness.

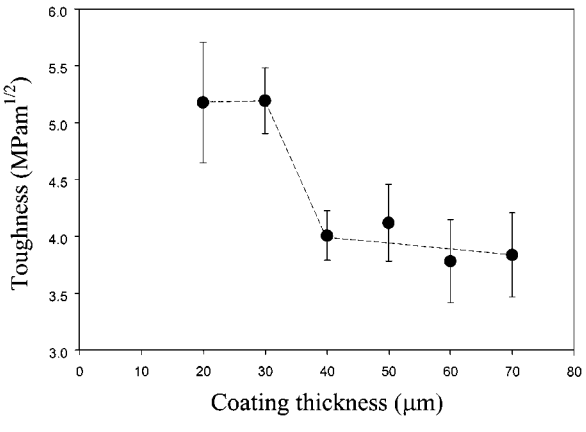

Figure 9 Toughness of SiC/graphite with coating thickness. Indentation at $P = 2$ N. Note abrupt increase of toughness at thinner coating thickness.

Subdamages are confirmed by the mechanical sectioning grinding. Indentation damage pattern exhibits only ring cracks and slight surface impression. According to the section grinding, the sizes of ring cracks increase and some microcracks are observed on the inside of inner ring crack. This indicates ring crack is unstable and propagates downward with maintaining some cone crack angle [3]. When the material is indented by a hard ball, at $P >$ Pc, cone cracks of length c are produced and propagated into the subsurface with maintaining constant cone crack angle. Some systems contain diffuse microdamage in the region of strong compression-shear beneath the contact [12, 28], which consists of shear-activated microcracks. The results of some more sectioning show no microcracks any longer. This result indicates that the microcracks are formed in the limited subdamage region which maximum shear stress is acted. Fig. 10b shows micrographs of top surface damage formed at the same indentation load in the specimen with 30 μm coating thickness. Contrary to the results of Fig. 10a, the ring crack suppression is manifest and much more surface impressions are observed. The size of damage zone also increases rather than the specimen with relatively thicker coating thickness. Sectioning results show that there are no cone cracks except microcracks in the damage zone.

4. Discussion

In this study we have characterized the SiC deposited on the graphite substrate by static indentation tests such as nanoindentation, microhardness indentation and Hertzian indentation. We have investigated the indentation damages formed in the SiC coating layer with different thicknesses on very softer graphite substrate. Preliminary adhesion test indicates this system has a relatively strong coating/substrate interface ($P_c > 100$ N), where applied loading energy can be absorbed into the substrate. The effect of residual stress might be ignored because the thermal expansion coefficient of the graphite substrate is similar to that of silicon carbide (Table I, $\alpha \approx 4.3 \times 10^{-6}/^{\circ}$C) and the systems were fabricated at the same temperature. The mechanical characterization of the coating and the substrate monolith indicates elastic moduli of the coating and the substrate layer show a large discrepancy each other, suggesting the existence of large elastic/plastic mismatch between the coating and the substrate layers. Large elastic/plastic mismatch can cause coating failure and limit the lifetime of the coating system [15]. Therefore the coating thickness should be designed on the aspect of elastic/plastic mismatch when the contact loading condition is important. Desirable coating thickness should be suggested in the coating system with large elastic/plastic mismatch.

In the SiC-coated graphite with two controlled thicknesses of 50 μm and 70 μm, the hardnesses at the lower applied load (less than 50 mN) were similar to each other (Fig. 3). At the same specimens, however, hardnesses at the higher applied load (0.5–20 N) show discrepancy with a decreasing tendency (Fig. 4). As an applied indentation load increases or the coating thickness

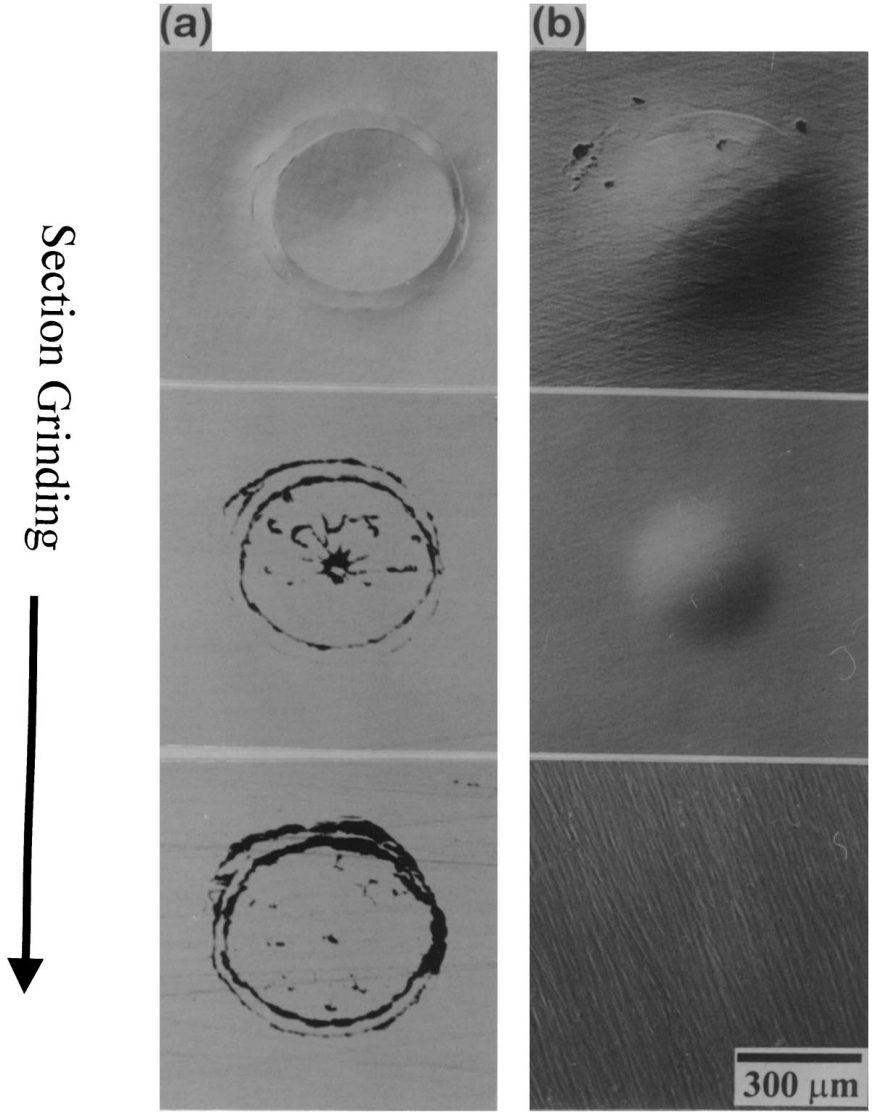

Figure 10 Micrographs of surface damage in SiC/graphite with different coating thickness; (a) $d = 70\ \mu$m and (b) $d = 50\ \mu$m after Hertzian indentation at load of 50 N with WC ball, $r = 3.18$ mm. The damages were observed with serial sectioning by polishing.

decreases, hardness shows much lower value. These results suggest that hardness is influenced by the characteristics of the substrate (Table I) as well as those of the coating layer in the hard coating/soft substrate system with strong interfacial bonding, which is more manifest as the applied indentation load increases or the coating thickness decreases.

These facts can also be confirmed in the evaluation of elastic modulus (Figs 7 and 8). For the specimens with 70 μm coating thickness, average elastic modulus at the lower applied load (less than 50 mN) by nanoindentation test is 460 GPa which is similar to that of the bulk SiC as shown in Table I. On the other hand, at the same specimens, elastic modulus at the higher applied load ($P > 25$ N) by the Hertzian test is 41.8 GPa. This difference of elastic modulus is seemed to result from the different damage areas of each indentation test. Submicron-scaled damage region is considered in nanoindentation test, so elastic modulus could be calculated from the load applied only on the coated layer. Therefore, effect of the characteristics of the substrate on the elastic modulus may be minimized. However, micrometer-scaled larger damage should be considered in Hertzian test. That is, in this test, larger ($r = 3.18$ mm) indenter was used to induce the surface damage, so the characteristics of the substrate with much smaller elastic modulus may affect the measurement of elastic modulus of this bilayer material. Therefore, elastic modulus obtained by Hertzian indentation test is smaller than that by nanoindentation test.

The another evidence of substrate effect can be found from the evaluation of abrupt decrease of hardness by microhardness indentation, which is observed in the range of 2 N to 10 N in Fig. 4. To understand the reason of abrupt hardness decrease, the indentation damages were investigated by SEM. While small indentation flaws ($2c \approx 10\ \mu$m) with radial cracks are observed at $P = 2$ N in the specimen with coating thickness of 50 μm (Fig. 5a), relatively large flaws ($2c \approx 100\ \mu$m) with only ring-like cracks are observed at $P = 3$ N (Fig. 5b). This difference of the flaw size suggests that the contact deformation is changed from plastic to elastic behavior as reported of the glasslike carbon system [32]. At lower applied load of less than 2 N, the brittleness is predominantly due to the characteristics of

the coating layer. However, the abrupt increase of the damage size at more than 3 N is thought to be resulted from an increasing effect of the soft characteristic of the graphite. Therefore, the change of deformation mechanism from plastic to elastic is expected to increase with decreasing the coating thickness. Considering the above results of hardness and elastic modulus of the SiC coated graphite, the coating thickness and the substrate characterisitc should be carefully designed because the design factor of coating thickness can have a vital influence on the damage resistance of coating system.

The soft substrate resulted in the crack suppression in the SiC/graphite system with thinner coating thickness. Fig. 9 illustrates the crack suppression phenomena found in this system. As the coating thickness decreases up to 40 μm, the appearance of crack propagation is not much changed. The large increase of fracture toughness in thin-coated systems (20 and 30 μm) indicates that the presence of the soft substrate layer inhibited the crack growth in microhardness indentation. The reason of the existence of critical coating thickness to suppress the crack is related with the size of surface indentation damages. The radial crack lengths produced on the systems at indentation load $P = 2$ N are almost constant, $2c \approx 20$ μm, for the coating thicknesses from 40 μm to 70 μm. The damage zone will be influenced by the soft substrate when the coating thickness is comparable to the damage zone size. Therefore, at the critical thickness, the fracture toughness abruptly increases by the effect of the soft substrate. Hertzian crack suppression was also found in the system with thinner coating thickness rather than thicker coating thickness. Fig. 10 explains the crack initiation could be also suppressed in the thinner coating thickness, $d = 30$ μm. Only slight ring crack is observed in the thinner coating thickness rather than the obvious popped-in ring cracks in the thicker coating thickness. However, the serial section grinding on the coating section shows that slight ring crack does not propagate into the sublayer in the thinner coating thickness. The result of Fig. 11 confirms the suppression of crack initiation in the specimen with very thin coating thickness, $d = 20$ μm. Ring crack was not initiated up to the indentation load $P = 200$ N, which is much larger value than those of the specimens with thicker coating thicknesses ($P_c \approx 50$–60 N). These results provide the possibility of energy absorption into the sublayer when the hard indenter is pressed. The expansion of damage zone rather than the formation of radial or ring cracks with decreasing coating thickness indicates that energy absorption has occurred, which suppresses the crack initiation and/or propagation from the applied indentation load. Since the system fabricated by LPCVD has a strong coating/substrate interface, it is possible that fracture energy is absorbed in the damage zone or substrate rather than at the interface, crack arrest than crack deflection, thus the ability to absorb the outer applied indentation energy [9–11, 14, 15].

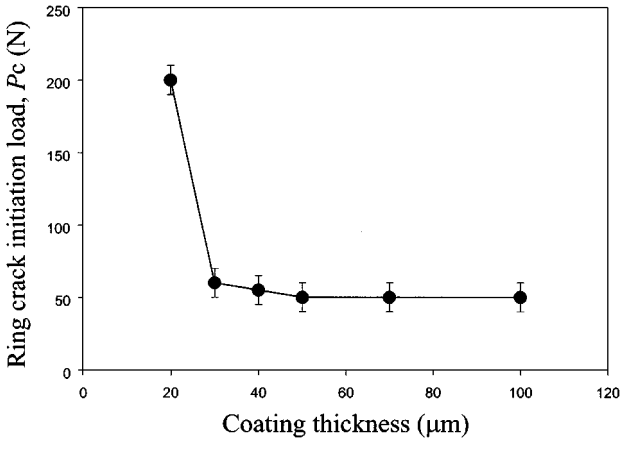

Figure 11 Critical loads Pc for ring crack initiation as a function of coating thickness for SiC/graphite system, WC sphere radius $r = 3.18$ mm.

These results suggest that the design of the coating thickness is important for coating or layer structure with large elastic/plastic mismatch between the coating and the substrate layers. To reduce the probability of coating fracture when the contact loading applies, thick coating thickness should be designed because the nature of the coating tensile stress is governed by the flexural stress with decreasing coating thickness. Therefore, a thick coating is favorable to prevent transverse fracture caused by elastic/plastic mismatch [15]. However, this study foreshadows another propose that very thin coating thickness might be favorable to prevent the crack initiation and/or propagation because of the damage absorption by the effect of the soft substrate. On the other hand, from the standpoint of hardness, thick coating is favorable for wear-resistant coating, which requires high hardness. The results of Fig. 3 indicate that silicon carbide grown on the graphite substrate by LPCVD has very high hardness. Thus, coating thickness should be designed on the aspect of material application. For instance, if wear-resistance is requiring property such as bearing or cutting tool, thick layer should be deposited while thin coating thickness is desirable for high toughness.

Ideally brittle homogeneous ceramics shows abrupt strength drop at the critical load for the formation of cone crack, while relatively ductile heterogeneous ceramics exhibits no strength loss [27]. Prior studies show that no strength degradation against the given contact static load indicates high damage tolerance of the material [11, 12, 27, 28]. Thus, it is expected that the effect of the soft substrate yields ultimately high damage tolerant system because of the crack suppression shown in this study.

5. Conclusion

Silicon carbide was deposited on the soft graphite substrate by LPCVD method. The coating thickness was controlled in the range of 20–70 μm. Various load was indented by nanoindentation, microhardness indentation and Hertzian indentation. The silicon carbide layer deposited on graphite substrate showed high hardness of $\approx$46 GPa and low toughness of 3.8 MPa $m^{1/2}$ at small indentation load, $P = 5$–33 mN. However, the hardness decreased as the indentation load increased. Indentation damage mode was changed from plastic to elastic deformation, which brings the abrupt decrease

of hardness below 20 GPa. This decreasing tendency was dependent on the coating thickness, in turn, hardness decreased more as the coating thickness was thinner. On the other hand, the toughness was improved as the coating thickness is thinner. In special, there was a critical thickness below that a large increase of toughness up to 5.2 MPa $m^{1/2}$ was observed. The increase of toughness was also accompanied by the suppression of crack initiation and propagation. The results indicate soft substrate greatly affects on the hardness and toughness of the SiC/graphite system fabricated in this study.

Acknowledgements

This project has been carried out under the Nuclear R&D Program by MOST. The authors wish to thank Dr. Han, Jun-Hee and Dr. Byun, Taek-Sang for helpness with indentation tests and for many discussions. Prof. Du Jin Choi, Mr. Wang Chae-Hyun and Lee Young-Jin in Yonsei University assisted with CVD processing.

References

1. B. R. LAWN, "Fracture of Brittle Solids" (Cambridge Univ. Press, Cambridge, 1993).
2. A. P. BORESI, R. J. SCHMIDT and O. M. SIDEBOTTOM, "Advanced Mechanics of Materials" (John Wiley & Sons, Inc., New York, 1993).
3. A. C. FISCHER-CRIPPS, "Introduction to Contact Mechanics" (Australia, 1996).
4. T. L. ANDERSON, "Fracture Mechanics" (CRC Press, London, 1995).
5. N. McN. ALFORD, J. D. BIRCHALL and K. KENDALL, *Nature* **330** (1987) 51.
6. N. P. PADTURE, S. J. BENNISON and H. M. CHAN, *J. Am. Ceram. Soc*. **76** (1993) 2312.
7. H. WANG and X. HU, *ibid*. **79** (1996) 553.
8. A. V. VIRKAR, J. L. HUANG and R. A. CUTLER, *ibid*. **70** (1987) 164.
9. S. WUTTIPHAN, B. R. LAWN and N. P. PADTURE, *ibid*. **79** (1996) 634.
10. L. AN., H. M. CHAN, N. P. PADTURE and B. R. LAWN, *J. Mater. Res*. **11** (1996) 204.
11. K. S. LEE, S. K. LEE, B. R. LAWN and D. K. KIM, *J. Am. Ceram. Soc*. **81** (1998) 2394.
12. S. K. LEE, S. WUTTIPHAN and B. R. LAWN, *ibid*. **80** (1997) 2367.
13. H. H. K. XU, L. WEI, N. P. PADTURE, B. R. LAWN and R. L. YECKLEY, *J. Mater. Sci*. **30** (1995) 869.
14. H. M. CHAN, *Ann. Rev. Mater. Sci*. **27** (1997) 249.
15. K. S. LEE, S. WUTTIPHAN, X. Z. HU, S. K. LEE and B. R. LAWN, *J. Am. Ceram. Soc*. **81** (1998) 571.
16. R. H. JONES, D. STEINER, H. L. HEINISCH, G. A. NEWSOME and H. M. KERCH, *J. Nucl. Mater*. **245** (1997) 87.
17. L. L. SNEAD, R. H. JONES, A. KOHYAMA and P. FENICI, *ibid*. **233–237** (1996) 26.
18. A. G. EVANS and J. W. HUTCHINSON, *Int. J. Solids Struc*. **20** (1984) 455.
19. W. J. CLEGG, K. KENDALL, N. M. ALFORD, T. W. BUTTON and J. D. BIRCHALL, *Nature* **347** (1991) 455.
20. J. C. KNIGHT, T. F. PAGE and I. M. HUTCHINGS, *Thin Solid Films* **177** (1989) 117.
21. W. C. OLIVER and G. M. PHARR, *J. Mater. Res*. **7** (1992) 1564.
22. K. ZENG and D. ROWCLIFFE, *Phil. Mag. A* **74** (1996) 1107.
23. X. LI, D. DIAO and B. BHUSHAN, *Acta. Mater*. **45** (1997) 4453.
24. D. TABOR, "Hardness of Metals" (Clarendon, Oxford, 1951).
25. D. B. MARSHALL, T. NOMA and A. G. EVANS, *J. Am. Ceram. Soc*. **65** (1982) C175.
26. F. GUIBERTEAU, N. P. PADTURE, H. CAI and B. R. LAWN, *Phil. Mag. A* **68** (1993) 1003.
27. B. R. LAWN, S. K. LEE, I. M. PETERSON and S. WUTTIPHAN, *J. Am. Ceram. Soc*. **81** (1998) 1509.
28. B. R. LAWN, *ibid*. **81** (1998) 1977.
29. B. R. LAWN and T. R. WILSHAW, *J. Mater. Sci*. **10** (1975) 1049.
30. X. Z. HU and B. R. LAWN, *Thin Solid Films* **322** (1998) 225.
31. A. PAJARES, L. WEI, B. R. LAWN, N. P. PADTURE and C. C. BERNDT, *Materials Sci. and Eng*. **A208** (1996) 158.
32. M. SAKAI, H. HANYU and M. INAGAKI, *J. Am. Ceram. Soc*. **78** (1995) 1006.

Received 30 March
and accepted 22 November 1999